

Investigation of the thermal effects on the nuclear matter

Ankit Kumar^{1,2} , H. C. Das^{1,2}, S. K. Biswal³, Bharat Kumar⁴, S. K. Patra^{1,2}, 

¹ Institute of Physics, Sachivalya Marg, Bhubaneswar-751005, India

² Homi Bhabha National Institute, Training School Complex, Anushakti Nagar, Mumbai 400085, India

³ Department of Astronomy, Xiamen University, Xiamen 361005, P. R. China

⁴ Center for Computational Sciences, University of Tsukuba, Tsukuba 305-8577, Japan

19 May 2020

ABSTRACT

We study the thermal effects on the nuclear matter properties such as binding energy, incompressibility, free symmetry energy and its coefficients using NL3 and G3 parameter sets of relativistic mean-field models. These models being consistent with the properties of cold nuclear matter, have also been used to study the effect of temperature by incorporating the Fermi function. The critical temperature for the liquid-gas phase transition in the symmetric nuclear matter is found to be 14.60 and 15.37 MeV for NL3 and G3 parameter sets respectively, which is in excellent agreement with previous theoretical and experimental studies. We inspect that the properties related to second differential coefficient of the binding energy and free symmetry energy at saturation density (i.e. $K_0(n, T)$ and $Q_{sym,0}$) exhibit the contrary effects for NL3 and G3 parameters as the temperature increases. We find that the prediction of saturated curvature parameter ($K_{sym,0}$) for G3 equation of state at finite temperature favour the combined analysis of $K_{sym,0}$ for the existence of massive pulsars, gravitational waves from GW170817 and NICER observations of PSR J0030+0451. Further, we investigate the cooling mechanism of newly born stars through neutrino emissivity controlled by direct Urca process and instate some interesting remarks about neutrino emissivity. We also deliberate the effect of temperature on the M-R profile of Proto-Neutron star.

Key words: nuclear matter—equation of state—stars: neutron—neutrinos

1 INTRODUCTION

One of the most prominent energetic events of the universe is manifested by the core-collapse supernovae (CCSN) explosion of the giant stars having mass in the range of 8 - 40 times that of the mass of sun (Gilmore 2004). The concept that the gravitational instability during the evolution of a massive star results in a rapid compression and then thermonuclear explosion, was first suggested by Burbidge, Burbidge, Fowler, and Hoyle (designated as “*B*²*FH*”) (Colgate & White 1966). The energy emerge during this explosion is carried off by the photons and the neutrinos, which are billion trillion trillion in numbers and hauled the most of the energy released. The observation of Einstein Observatory (HEAO-2) first supported the fact that high neutrino emissivity is mainly responsible for the rapid cooling of newly born dense star (Boguta 1981). Studies suggest that the neutrinos also play a significant

role in the dynamics of supernovae explosion and control many important aspects of the collapsed core, generally known as newly born neutron star (Burrows 2000; Ryden 2003). In this exploring era of every tiny and massive object through modern science, neutron stars still hold the mystery in itself and are poorly known objects. These are the ideal playfield in the observable universe to inspect the theories of dense matter physics and unfold new opportunities. A large part of our perception about the dynamics of supernovae explosion and the composition of neutron stars is based on the equation of state (EoS), which makes the EoS a key ingredient of our study. Since it is believed that the matter evolved during the core-collapse phenomenon is unable to attain β -equilibrium condition for few seconds (Stone & Reinhard 2007), due to the promptness of the CCSN explosion, so, usually the EoS for a dense matter with either same amount of protons and neutrons or a proton fraction of ~ 0.2 is taken into account to cipher the dynamics of collapse event (Mezzacappa 2005). Many other important aspects of core collapse events like how many protons are converted into neutrons, quenching rate,

* E-mail: ankit.k@iopb.res.in

† patra@iopb.res.in

the mass-radius profile of newly born neutron star and its composition are determined by the EoS (Schneider et al. 2019).

Another important dimension which makes the EoS of nuclear matter (NM) at finite temperature more interesting is the study of the dynamics of heavy ion collision reaction and structure of exotic nuclei. Under extreme conditions of density, isospin and temperature the EoS can be explored through many experimental facilities such as GANIL-SPIRAL2 (Facilities Facilities) facility in France, CSR in China (Zhan et al. 2006) and the FRIB technique in the United States (FRIB FRIB). Nuclear collisions can produce hot and dense hadronic NM in terrestrial laboratories momentarily, which can procure a lot of information about the thermodynamical properties of NM like incompressibility, symmetry energy and its derivatives (Danielewicz et al. 2002). In heavy-ion collision experiments, the symmetry energy plays an important role in understanding the isoscaling behaviour of multi-fragmentation phenomena. The observations of the experiments at Texas A&M University and National Superconducting Cyclotron Laboratory suggest a connection between the nuclear symmetry energy and primary fragment yield distribution of statistical multi-fragmentation model (Ono et al. 2003; Souliotis et al. 2006; Iglio et al. 2006). On the other hand, symmetry energy at finite temperature also plays an important role in the cooling mechanism of newly born hot astrophysical objects (Prakash et al. 1997; Takatsuka 1996; Li et al. 2008) and has effective impact on the cooling rate through direct Urca and modified Urca processes (Yakovlev & Levenfish 1995; Gusakov, M. E. 2002).

In the recent years, the density dependence of the symmetry energy and its derivatives (L_{sym} , K_{sym} , Q_{sym}) have been used to constrain the EoS near saturation density, which make them more vital to decipher properly. It is well known that the slope parameter (L_{sym}) and the size of the neutron skin in super-heavy nuclei are connected by a strong linear correlation. The slope (L_{sym}) and curvature parameter (K_{sym}) also control the location of the neutron drip line, core-crust transition density and gravitational binding energy of neutron star (Tsang et al. 2019). The isovector skewness parameter (Q_{sym}) is the most ambiguous quantity, due to the large fluctuations in its value obtained from different models. Recent studies show that Q_{sym} is related to the incompressibility (Typel 2018) of the system and also suggest an important role of Q_{sym} in the cooling of newly born proto-neutron star (Schneider et al. 2019). We study in detail the effects of temperature on all these nuclear parameters and the correlations among them using the most familiar NL3 and recently developed G3 parameter sets.

In the extant work, we also investigate the dependence of cooling mechanism of a hot dense matter on the EoS and the variation in the mass-radius profile of a proto-neutron star with temperature. The temperature in the interior of a newly born dense star just after the supernova explosion can vary from 10 to 100 MeV (Oechslin, R. et al. 2007). The analysis of the x-rays emitted during the stellar evolution of the young star ensure the fact that it losses

most of its energy through extremely rapid neutrino emission enhanced by the direct Urca process (named after a casino in Rio) (Brown et al. 2018a; Kaminker, A. D. et al. 2001; Yakovlev & Pethick 2004). However, the direct Urca process dominates only during the initial stage of the cooling and can no longer operate once the proton fraction inside the core reaches a threshold value. The proton fraction in a newly born proto-neutron star depends on how the nuclear symmetry energy scales with density – which is an important aspect of this work (Brown et al. 2018a). In the mean field approximation, the symmetry energy and the magnitude of the neutrino emissivity (Q) seem to be controlled by the EoS of different parameter sets.

The paper is organized as: In section 2, we explain the formalism for temperature dependent quantum hadrodynamics model. Section 3 is divided into two parts, where 3.1 is devoted to the theoretical structure of the relativistic mean field formalism at finite temperature and acquaintance with the NM parameters. In sub-section 3.2 we presented the results for various NM parameters of symmetric NM using NL3 and G3 parameter sets. The detailed framework and the results of neutrino emissivity through direct Urca process are extended in section 4. The mass-radius profile of proto-neutron star is discussed in section 5. Finally the discussion and the concluding remarks are outlined in the section 6.

2 TEMPERATURE DEPENDENT QHD MODEL

Temperature dependent QHD model is based on relativistic covariant field theory, proposed to obtain the exponential in-medium nuclear properties around the saturation density. The nucleons (neutrons and protons) are represented by the Dirac spinor ψ in the Lagrangian density. We take in account the σ , ω , ρ and δ mesons in our Lagrangian, represented by the σ , ω^μ , $\vec{\rho}^\mu$ and $\vec{\delta}$ fields respectively. The mesons act as the mediators and represent the effective nuclear interaction of the nucleons through the meson fields σ , ω^μ , $\vec{\rho}^\mu$ and $\vec{\delta}$. The basic Lagrangian density used in the present work, which includes the interaction of nucleon fields ψ with a scalar field (σ), a vector field (ω) and isovector fields ($\vec{\rho}^\mu$ and $\vec{\delta}$) and the cross-coupled interactions of these meson fields upto

fourth order (Singh et al. 2014), is given by

$$\begin{aligned} \mathcal{L} = & \sum_{\alpha=p,n} \bar{\psi}_\alpha \left\{ \gamma_\mu (i\partial^\mu - g_\omega \omega^\mu - \frac{1}{2} g_\rho \vec{\tau}_\alpha \cdot \vec{\rho}^\mu) - (M - g_\sigma \sigma \right. \\ & \left. - g_\delta \vec{\tau}_\alpha \cdot \vec{\delta}) \right\} \psi_\alpha + \frac{1}{2} \left(\partial^\mu \sigma \partial_\mu \sigma - m_\sigma^2 \sigma^2 \right) + \frac{\zeta_0}{4!} g_\omega^2 (\omega^\mu \omega_\mu)^2 \\ & - g_\sigma \frac{m_\sigma^2}{M} \left(\frac{\kappa_3}{3!} + \frac{\kappa_4}{4!} \frac{g_\sigma}{M} \sigma \right) \sigma^3 + \left(\frac{1}{2} m_\omega^2 \omega^\mu \omega_\mu - \frac{1}{4} F^{\mu\nu} F_{\mu\nu} \right) \\ & + \frac{1}{2} \frac{g_\sigma \sigma}{M} \left(\eta_1 + \frac{\eta_2}{2} \frac{g_\sigma \sigma}{M} \right) m_\omega^2 \omega^\mu \omega_\mu + \frac{1}{2} \eta_\rho \frac{m_\rho^2}{M} g_\sigma \sigma (\vec{\rho}^\mu \cdot \vec{\rho}_\mu) \\ & + \left(\frac{1}{2} m_\rho^2 \rho^\mu \cdot \rho_\mu - \frac{1}{4} \vec{R}^{\mu\nu} \cdot \vec{R}_{\mu\nu} \right) - \Lambda_\omega g_\omega^2 g_\rho^2 (\omega^\mu \omega_\mu) (\vec{\rho}^\mu \cdot \vec{\rho}_\mu) \\ & + \frac{1}{2} \left(\partial^\mu \vec{\delta} \partial_\mu \vec{\delta} - m_\delta^2 \vec{\delta}^2 \right), \end{aligned} \quad (1)$$

where M is the nucleon mass; m_σ , m_ω , m_ρ and m_δ are the masses of mesons and g_σ , g_ω , g_ρ and g_δ are the coupling constants for the σ , ω , ρ and δ mesons respectively; κ_3 (or κ_4) and ζ_0 are the self-interacting coupling constants of the σ and ω mesons respectively; η_1 , η_2 , η_ρ and Λ_ω are the coupling constants of non-linear cross-coupled terms. The quantities $F^{\mu\nu}$ and $\vec{R}^{\mu\nu}$ being the field strength tensors for the ω and ρ mesons respectively, defined as $F^{\mu\nu} = \partial^\mu \omega^\nu - \partial^\nu \omega^\mu$ and $\vec{R}^{\mu\nu} = \partial^\mu \vec{\rho}^\nu - \partial^\nu \vec{\rho}^\mu$. The $\vec{\tau}$ are the Pauli matrices and behave as the isospin operator, which carry the isospin component of the nucleons.

In the further calculations of the present work, we will consider relativistic mean field approximation and isotropy in isospin space. Within the assumed approximation, the meson fields are replaced by their expectation values and for rotationally invariant systems only the time component ($\mu = 0$) of the isovector field survives (Aguirre 2012; Liu et al. 2002). The third component of the isospin operator (τ_3) when operates on neutron and proton gives, $\tau_3 |p\rangle = (+1) |p\rangle$ and $\tau_3 |n\rangle = (-1) |n\rangle$. Applying the relativistic mean-field approximation, the Lagrangian density yields the following Dirac equation for the nucleon field

$$\left\{ i\gamma_\mu \partial^\mu - g_\omega \gamma_0 \omega - \frac{1}{2} g_\rho \gamma_0 \tau_3 \alpha \rho - M_\alpha^* \right\} \psi_\alpha = 0, \quad (2)$$

where M_α^* is the effective mass of the nucleon. Taking into account the third component of the isospin for neutron and proton as defined above, the effective masses of the neutron and proton are given by

$$M_p^* = M - g_s \sigma - g_\delta \delta, \quad (3)$$

$$M_n^* = M - g_s \sigma + g_\delta \delta, \quad (4)$$

The Lagrangian density can be used to derive Euler-Lagrange equations of motion for the meson fields with the help of relativistic mean field approximation as

(Kumar et al. 2018)

$$\begin{aligned} m_\sigma^2 \sigma &= g_\sigma \sum_{\alpha=p,n} \langle \bar{\psi}_\alpha \gamma_0 \psi_\alpha \rangle - \frac{m_\sigma^2 g_\sigma}{M} \sigma^2 \left(\frac{\kappa_3}{2} + \frac{\kappa_4}{3!} \frac{g_\sigma \sigma}{M} \right) \\ &+ \frac{g_\sigma}{2M} \left(\eta_1 + \eta_2 \frac{g_\sigma \sigma}{M} \right) m_\omega^2 \omega^2 + \frac{\eta_\rho}{2M} g_\sigma m_\rho^2 \rho^2, \end{aligned} \quad (5)$$

$$\begin{aligned} m_\omega^2 \omega &= g_\omega \sum_{\alpha=p,n} \langle \bar{\psi}_\alpha \psi_\alpha \rangle - \left(\eta_1 + \frac{\eta_2}{2} \frac{g_\sigma \sigma}{M} \right) \frac{g_\sigma \sigma}{M} m_\omega^2 \omega \\ &- \frac{1}{3!} \zeta_0 g_\omega^2 \omega^3 - 2 \Lambda_\omega g_\omega^2 g_\rho^2 \rho^2 \omega, \end{aligned} \quad (6)$$

$$\begin{aligned} m_\rho^2 \rho &= \frac{1}{2} g_\rho \sum_{\alpha=p,n} \langle \bar{\psi}_\alpha \tau_3 \psi_\alpha \rangle - \eta_\rho \frac{g_\sigma \sigma}{M} m_\rho^2 \rho \\ &- 2 \Lambda_\omega g_\omega^2 g_\rho^2 \omega^2 \rho, \end{aligned} \quad (7)$$

$$m_\delta^2 \delta = g_\delta \sum_{\alpha=p,n} \langle \bar{\psi}_\alpha \tau_3 \gamma_0 \psi_\alpha \rangle. \quad (8)$$

Assuming NM as an uniform system, where the fields of σ , ω and ρ mesons are independent of position and taking the thermodynamic argument of free gas into consideration, the baryon, scalar and isovector densities for the appropriate Fermi momentum at finite temperature can be evaluated as (Wang 2000; Yang et al. 2019a; Kumar et al. 2018)

$$\begin{aligned} n &= \sum_{\alpha=p,n} \langle \bar{\psi}_\alpha \psi_\alpha \rangle = n_p + n_n \\ &= \sum_{\alpha=p,n} \frac{2}{(2\pi)^3} \int_0^{k_\alpha} d^3 k [f_\alpha(\mu_\alpha^*, T) - \bar{f}_\alpha(\mu_\alpha^*, T)], \end{aligned} \quad (9)$$

$$\begin{aligned} n_s &= \sum_{\alpha=p,n} \langle \bar{\psi}_\alpha \gamma_0 \psi_\alpha \rangle = n_{sp} + n_{sn} \\ &= \sum_{\alpha=p,n} \frac{2}{(2\pi)^3} \int_0^{k_\alpha} d^3 k \frac{M_\alpha^*}{(k_\alpha^2 + M_\alpha^{*2})^{\frac{1}{2}}} \\ &\left[f_\alpha(\mu_\alpha^*, T) + \bar{f}_\alpha(\mu_\alpha^*, T) \right], \end{aligned} \quad (10)$$

$$n_3 = \sum_{\alpha=p,n} \langle \bar{\psi}_\alpha \tau_3 \psi_\alpha \rangle = n_p - n_n, \quad (11)$$

$$n_{s3} = \sum_{\alpha=p,n} \langle \bar{\psi}_\alpha \tau_3 \gamma_0 \psi_\alpha \rangle = n_{sp} - n_{sn}, \quad (12)$$

where n_p and n_n are the proton and neutron densities respectively, k_α is the nucleon Fermi momentum, T is the temperature, $f_\alpha(\mu_\alpha^*, T)$ and $\bar{f}_\alpha(\mu_\alpha^*, T)$ are the thermal Fermi distribution function of the nucleon and the anti-nucleon, and μ_α^* is the effective chemical potential of the nucleon. The familiar Fermi distribution function for the particle and the anti-particle can be written as (Wang 2000)

$$f_\alpha(\mu_\alpha^*, T) = \frac{1}{e^{(\mathcal{E}_\alpha^* - \mu_\alpha^*)/k_B T} + 1}, \quad (13)$$

$$\bar{f}_\alpha(\mu_\alpha^*, T) = \frac{1}{e^{(\mathcal{E}_\alpha^* + \mu_\alpha^*)/k_B T} + 1}, \quad (14)$$

where k_B is the Boltzmann constant and \mathcal{E}_α^* is the effective energy of the nucleon which can be written as

$$\mathcal{E}_\alpha^* = \sqrt{k_\alpha^2 + M_\alpha^{*2}}. \quad (15)$$

The effective chemical potential of the proton and the neu-

tron can be derived as (Wang 2000)

$$\mu_p^* = \mu_p - g_\omega \omega - \frac{1}{2} g_\rho \rho, \quad (16)$$

$$\mu_n^* = \mu_n - g_\omega \omega + \frac{1}{2} g_\rho \rho, \quad (17)$$

where μ_p and μ_n are the usual the chemical potential of proton and neutron relative to free nucleon mass.

3 SYMMETRIC NUCLEAR MATTER

3.1 Theoretical Formalism

In the following section, the formalism used for the calculations of symmetric and asymmetric NM properties has been discussed. To describe the asymmetric NM, we introduce the asymmetric parameter t , which is defined as,

$$t = \frac{n_n - n_p}{n_n + n_p}. \quad (18)$$

We can assign the desired asymmetry in the nuclear matter by varying the value of t . For symmetric NM (SNM), $t = 0$ and $t = 1$ for pure neutron matter. In the present work, we extend our calculations for SNM ($t = 0$). The energy density and the pressure for the NM can be calculated from the Lagrangian using the expression for energy-momentum tensor (Fetter & Walecka 1971), which is

$$T^{\mu\nu} = \sum_j \frac{\partial \mathcal{L}}{\partial (\partial_\mu \phi_j)} \partial^\nu \phi_j - \eta^{\mu\nu} \mathcal{L}, \quad (19)$$

where ϕ_j includes all the fields present in the Lagrangian. Using this expression of the energy density and pressure for a warm nuclear system can be naively derived as (Singh et al. 2014)

$$\begin{aligned} E = & \sum_{\alpha=p,n} \frac{2}{(2\pi)^3} \int_0^{k_\alpha} d^3 k \mathcal{E}_\alpha^*(k) \left[f_\alpha(\mu_\alpha^*, T) + \bar{f}_\alpha(\mu_\alpha^*, T) \right] \\ & + n g_\omega \omega + m_\sigma^2 \sigma^2 \left(\frac{1}{2} + \frac{\kappa_3}{3!} \frac{g_\sigma \sigma}{M} + \frac{\kappa_4}{4!} \frac{g_\sigma^2 \sigma^2}{M^2} \right) \\ & - \frac{1}{2} m_\omega^2 \omega^2 \left(1 + \eta_1 \frac{g_\sigma \sigma}{M} + \frac{\eta_2}{2} \frac{g_\sigma^2 \sigma^2}{M^2} \right) - \frac{1}{4!} \zeta_0 g_\omega^2 \omega^4 \\ & + \frac{1}{2} n_3 g_\rho \rho - \frac{1}{2} \left(1 + \frac{\eta_\rho g_\sigma \sigma}{M} \right) m_\rho^2 \rho^2 \\ & - \Lambda_\omega g_\rho^2 g_\omega^2 \rho^2 \omega^2 + \frac{1}{2} m_\delta^2 \delta^2, \end{aligned} \quad (20)$$

and

$$\begin{aligned} P = & \sum_{\alpha=p,n} \frac{2}{3(2\pi)^3} \int_0^{k_\alpha} d^3 k \frac{k^2}{\mathcal{E}_\alpha^*(k)} \left[f_\alpha(\mu_\alpha^*, T) + \bar{f}_\alpha(\mu_\alpha^*, T) \right] \\ & - m_\sigma^2 \sigma^2 \left(\frac{1}{2} + \frac{\kappa_3}{3!} \frac{g_\sigma \sigma}{M} + \frac{\kappa_4}{4!} \frac{g_\sigma^2 \sigma^2}{M^2} \right) + \frac{1}{4!} \zeta_0 g_\omega^2 \omega^4 \\ & + \frac{1}{2} m_\omega^2 \omega^2 \left(1 + \eta_1 \frac{g_\sigma \sigma}{M} + \frac{\eta_2}{2} \frac{g_\sigma^2 \sigma^2}{M^2} \right) + \Lambda_\omega g_\rho^2 g_\omega^2 \rho^2 \omega^2 \\ & + \frac{1}{2} \left(1 + \frac{\eta_\rho g_\sigma \sigma}{M} \right) m_\rho^2 \rho^2 - \frac{1}{2} m_\delta^2 \delta^2. \end{aligned} \quad (21)$$

Since we deal with the temperature dependent NM, we also did some study regarding phase coexistence, which unfolds

the liquid-gas phase transition in thermal NM. The NM system can remain only in one phase (gaseous) once it reaches the critical point (Wang 2000). For symmetric NM, the inflection point of the pressure curve with respect to the total nucleon density determines the critical point (Yang et al. 2019a), that is

$$\left. \frac{\partial P}{\partial n} \right|_{T=T_C} = \left. \frac{\partial^2 P}{\partial n^2} \right|_{T=T_C} = 0, \quad (22)$$

T_C being the critical temperature. One of the basic and fundamental quantity of the NM is incompressibility, also known as the isoscalar incompressibility or compression modulus (K) (Schneider et al. 2019). K directly influences the curvature of the equation of state and gives adequate information about the nature of the equation of state. Higher the value of K , more stiff the equation of state will be (Tan et al. 2016). The incompressibility is related to the equation of state through (Fetter & Walecka 1971)

$$K(n, T) = 9 n^2 \frac{\partial^2 (E/n)}{\partial n^2}. \quad (23)$$

Another important quantity which controls the equation of state of NM is symmetry energy. Symmetry energy has a significant contribution to the pressure of the astrophysical objects which is responsible for gravitational attraction (Goudarzi et al. 2018). In case of the hot NM, we can define two forms of symmetry energy, one we call as the nuclear symmetry energy (E_{sym}) and the other as free symmetry energy (F_{sym}). In order to calculate the free symmetry energy of the hot NM, we need entropy density S and free energy density F of that system. So the the free energy density is given by

$$F = E - TS, \quad (24)$$

and the entropy density for a hot NM is calculated by (Fetter & Walecka 1971)

$$\begin{aligned} S = & - \sum_{\alpha=p,n} \frac{2}{(2\pi)^3} \int_0^{k_\alpha} d^3 k \left[f_\alpha(\mu_\alpha^*, T) \ln f_\alpha(\mu_\alpha^*, T) \right. \\ & \left. + (1 - f_\alpha(\mu_\alpha^*, T)) \ln (1 - f_\alpha(\mu_\alpha^*, T)) + \bar{f}_\alpha(\mu_\alpha^*, T) \right. \\ & \left. \ln \bar{f}_\alpha(\mu_\alpha^*, T) + (1 - \bar{f}_\alpha(\mu_\alpha^*, T)) \ln (1 - \bar{f}_\alpha(\mu_\alpha^*, T)) \right] \end{aligned} \quad (25)$$

Various theoretical studies have shown that we can calculate the temperature and density dependence of nuclear symmetry energy in hot symmetric NM using empirical parabolic approximation, which can be estimated as the difference of the energy per nucleon of pure neutron matter and symmetric NM (Tan et al. 2016). In the similar way, we can find the free symmetric energy for a hot NM, which is of utmost importance for astrophysical phenomena. The free symmetric energy of a symmetric NM can be defined as (Tan et al. 2016; Li et al. 2008)

$$F_{sym}(n, T) = \frac{F(n, T, t=1)}{n} - \frac{F(n, T, t=0)}{n}, \quad (26)$$

which can be interpreted as the remnant of free energy per nucleon for pure neutron matter and symmetric NM.

The free symmetry energy can be expanded in a Taylor series expansion around χ . It is a dimensionless variable which describes the density deviation from saturation

density and for mathematical convention and simplification of the expressions of higher order derivatives defined as, $\chi = (n - n_0)/3n_0$, n_0 being the saturation density. So the expansion can be written as,

$$F_{sym}(n, T) = F_{sym}(n_0) + L_{sym} \chi + \frac{K_{sym}}{2!} \chi^2 + \frac{Q_{sym}}{3!} \chi^3 + O(\chi^4), \quad (27)$$

where L_{sym} , K_{sym} and Q_{sym} are the slope parameter, curvature parameter and skewness parameter respectively. Recently it is convinced that these parameters are of utmost importance in nuclear and astrophysics by showing the correlation of these parameters with different nuclear and astrophysical properties (Schneider et al. 2019). The expressions for these parameters can be extracted as (Chen et al. 2009)

$$L_{sym}(n, T) = 3n \frac{\partial F_{sym}(n, T)}{\partial n}, \quad (28)$$

$$K_{sym}(n, T) = 9n^2 \frac{\partial^2 F_{sym}(n, T)}{\partial n^2}, \quad (29)$$

$$Q_{sym}(n, T) = 27n^3 \frac{\partial^3 F_{sym}(n, T)}{\partial n^3}. \quad (30)$$

Although we extract the results from this expansion at high densities, but we should not exclude the fact that at very high nuclear densities the error bar in higher order coefficients extracted through series expansion is quite high (Schneider et al. 2019).

3.2 Results

Throughout our calculations in this paper, we use NL3 and G3 parameter sets, where NL3 endue us the stiff EoS and G3 facilitate us to examine the softer region. The obtained results for the variation in the properties of the NM with temperature and density are discussed in the present section. The coupling constants and the empirical values of nuclear properties at saturation of cold EoS for both the parameter sets (NL3 and G3) are given in Table 1 (Lalazissis et al. 1997; Kumar et al. 2017). We start our discussion with the energy and pressure of hot NM and procurement of critical temperature for liquid-gas phase transition. In Fig.1 we depicted the calculated results of binding energy per nucleon and pressure density from $T = 0$ to 20 MeV as a function of density. We observed an increase in the binding energy and saturation density of the SNM with temperature for both NL3 and G3 parameter sets. The marked point on each curve of the upper panel of the Fig.1 represents its minima. It has been already reported that NM saturates around 0.148 fm^{-3} with binding energy per nucleon around -16 MeV for both the parameter sets at zero temperature (Kumar et al. 2018; Sakuragi 2016). Here we found that as we increase the temperature from 0 to 20 MeV, n_0 increases linearly from 0.148 to 0.196 fm^{-3} and similarly the binding energy also goes on increasing which is clear from the Fig.1. The increase in the binding energy per nucleon with temperature indicates that the system becomes more loosely bound at higher temperature.

Lower panel of Fig.1 shows the variation of pressure with temperature as a function of density. This adaptation

Table 1. The coupling constants and the NM properties at saturation for cold EoS of NL3 (Lalazissis et al. 1997) and G3 (Kumar et al. 2017) parameter sets. The nucleon mass (M) is 939.0 MeV. All of the coupling parameters are dimensionless and the NM parameters are in MeV, except k_3 and n_0 which are in fm^{-1} and fm^{-3} respectively. The NM parameters are given at saturation point for NL3 and G3 parameter sets in the lower panel.

	NL3	G3
m_σ/M	0.541	0.559
m_ω/M	0.833	0.832
m_ρ/M	0.812	0.820
m_δ/M	0.0	1.043
$g_\sigma/4\pi$	0.813	0.782
$g_\omega/4\pi$	1.024	0.923
$g_\rho/4\pi$	0.712	0.962
$g_\delta/4\pi$	0.0	0.160
k_3	1.465	2.606
k_4	-5.688	1.694
ζ_0	0.0	1.010
η_1	0.0	0.424
η_2	0.0	0.114
η_ρ	0.0	0.645
Λ_ω	0.0	0.038
n_0	0.148	0.148
$B.E.$	-16.29	-16.02
K_0	271.38	243.96
$F_{sym,0}$	37.43	31.84
$L_{sym,0}$	120.65	49.31
$K_{sym,0}$	101.34	-106.07
Ω	177 fm^{-3}	115 fm^{-3}

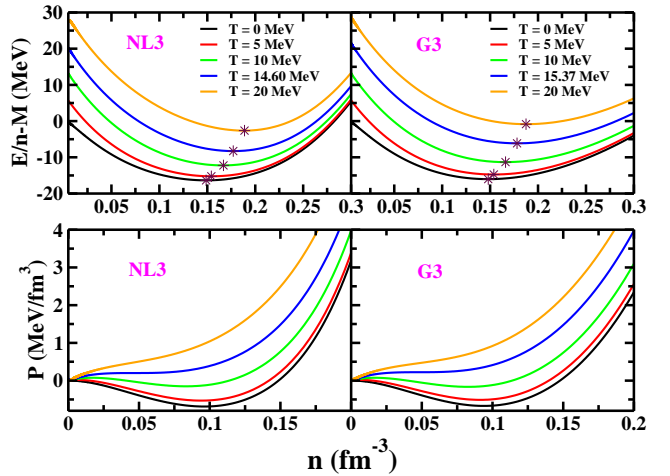


Figure 1. (colour online) Binding energy and pressure as a function of nucleon density for symmetric NM at different temperatures. The left and right panels show the results for NL3 and G3 parameter sets respectively.

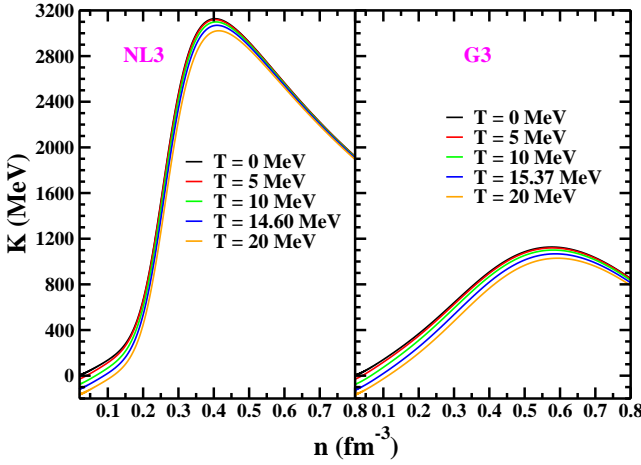


Figure 2. (colour online) Incompressibility (K) as a function of nucleon density for SNM ($t = 0$). The left panel shows the results for NL3 and right panel for G3 parameter set.

of pressure is utterly important in determining the critical parameters of liquid-gas phase transition specially the critical temperature, T_C . Various theoretical and experimental studies predict the value of T_C for SNM in the range of 10 – 20 MeV (Sharma & Pal 2010; Kāijpper et al. 1974; Yang et al. 2019b; Elliott et al. 2013; Takatsuka 1985). We also found the value of T_C using equation 22 as 14.60 and 15.37 MeV for NL3 and G3 parameter sets respectively. Other important characteristics quantities of the liquid-gas phase transition like P_C, ρ_C can also be determined using T_C with the help of correlations derived in reference (Yang et al. 2019b). The variation of the incompressibility modulus has also been depicted in Fig. 2 and 3. As the value of n increases, the chart of K exhibits an anomalous behaviour. We observed that the magnitude of K shows a maxima around 4 – 5 times of the saturation density for both the parameter sets. However the magnitude of K is quite high for NL3 parameter set in comparison to G3, which indicates a strong dependence of K on the nature of the EoS. We also observed an unfamiliar proneness in the K values at saturation density (denoted as K_0) for different temperature which are shown in Fig. 3. For NL3 parameter set K_0 shows an increment with increase in temperature while for G3 parameter set the case is reversed. This contemplation of K_0 confirms the sensitiveness of incompressibility on the choice of parametrization and the cross-coupling of field variables responsible for the softening of EoS. This fact has also been supported by the study in reference (Mekjian et al. 2005). We also analysed that the G3 parameter set indulge all the constraints of the elliptic flow heavy-ion collision experiment (Wang et al. 2018) on the value of K_0 , which is $K_0 = 220 \pm 40$ MeV. NL3, on the other hand, being the stiff parameter set depicts the higher value of K_0 and does not support the experimental results. The effect of the temperature on free symmetry energy and its derivatives has also been studied from lower to higher density of NM. Fig. 4 reflects the effect of temperature on F_{sym} and its first derivative L_{sym} (i.e slope parameter) of SNM. Rise in temperature does not hint any significant change in the symmetry energy of the system at high density. However, the magnitude of the symmetry energy at saturation density ($F_{sym,0}$) increases as we

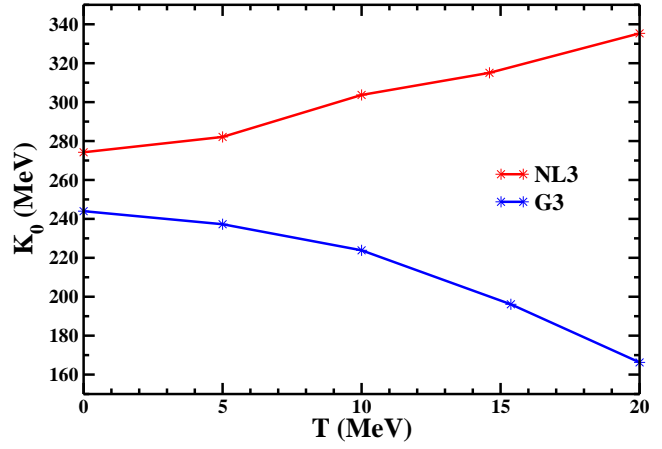


Figure 3. (colour online) Variation of incompressibility at sat-

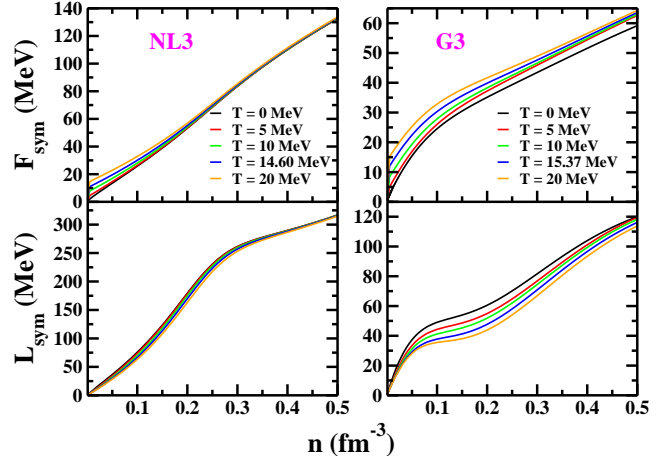


Figure 4. (colour online) Symmetry energy (F_{sym}) and L_{sym} as a function of nucleon density for SNM ($t = 0$). The left panel shows the results for NL3 and right panel for G3 parameter set.

increase the temperature. Another important aspect that we observed here is the difference in the magnitude of the F_{sym} for NL3 and G3 parameter sets. The magnitude range of F_{sym} for NL3 is quite high in comparison to G3, which indicates that the stiff EoS allocate higher value of symmetry energy. Again the determination of higher value of $F_{sym,0}$ along with K_0 by NL3 forces suggested that we need a better parameterized EoS, so that we can match the prediction of nuclear parameters made by various theoretical and experimental studies. On the other hand, the spectrum of F_{sym} at finite temperature determined by our recently developed G3 parameter, fall in the expected range which is verified by other studies also (Ou et al. 2011; Agrawal et al. 2014; Baldo & Burgio 2016; Burrello et al. 2019). L_{sym} changes slightly as we change the temperature for G3 parameter set, while for NL3 it remains unaffected. The change in slope parameter at saturation density ($L_{sym,0}$) with temperature is shown in Fig. 5. The effect of temperature on the second and third derivatives of F_{sym} , which are known as curvature and isovector skewness parameter respectively (denoted by K_{sym} and Q_{sym}) is shown in Fig. 6 and 7 for both the parameter sets. The variation of K_{sym} and Q_{sym} with

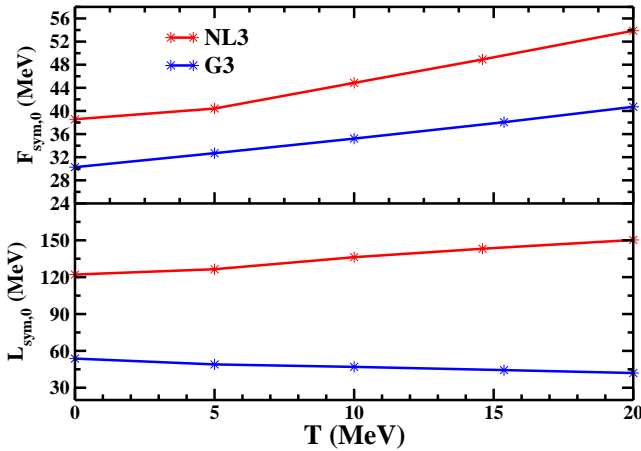


Figure 5. (colour online) Variation of symmetry energy and slope parameter at saturation density ($F_{sym,0}$ and $L_{sym,0}$) with temperature for SNM.

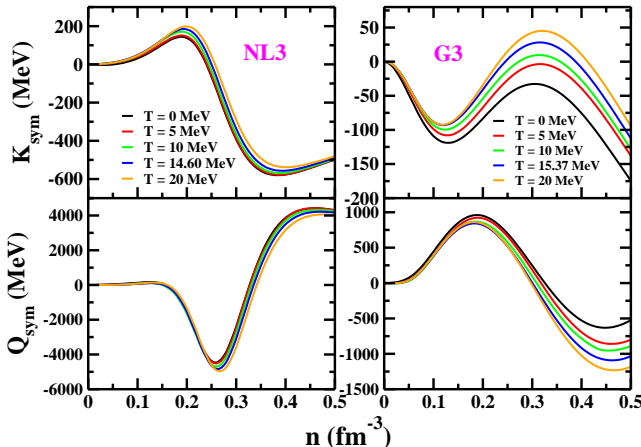


Figure 6. (colour online) K_{sym} and Q_{sym} as a function of nucleon density for SNM ($t = 0$). The left panel shows the results for NL3 and right panel for G3 parameter set.

density somehow reflects the sight of the sinusoidal wave, with extremum of the curve near twice the saturation density as can be seen in Fig. 6. K_{sym} , being the higher order parameter, can be constrained with the help of neutron star observations (Zimmerman et al. 2020). Recently, a study done by Josef Zimmerman et al. merged the data reported by two most vital experiments (PSR J0030+0451 by NICER Collaboration (Riley et al. 2019) and GW170817 by LIGO/Virgo (Abbott et al. 2017, 2018)) and derive a joint $1-\sigma$ constraint on curvature parameter at saturation density ($K_{sym,0}$). It is believed to be the most reliable bound on $K_{sym,0}$ till date and reported within the 90 % confident bounds as $K_{sym,0} = -102^{+71}_{-72}$ MeV (Zimmerman et al. 2020). In Fig. 7 we can see that the value of $K_{sym,0}$ estimated by G3 parameter set for entire temperature spectrum falls into the range of $1-\sigma$ constraint discussed above. NL3 parameter set, on the other hand, not only inconsistent with the estimated constraint but surprisingly falls entirely in the opposite magnitude range. This observation clearly reject the NL3 phenomenological model in determining the NM parameters for astrophysical observations and hints for G3 EoS, best suited

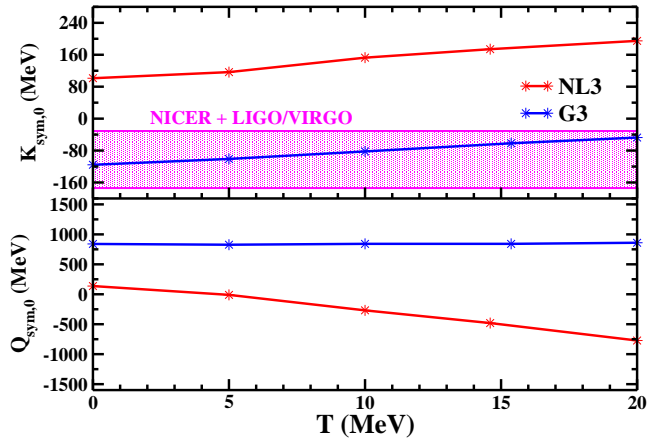


Figure 7. (colour online) Variation of Curvature parameter and Skewness parameter at saturation density ($K_{sym,0}$ and $Q_{sym,0}$, respectively) with temperature for SNM.

for the study of astrophysical phenomena. Studies show that there is a strong correlation between $K_{sym,0}$, tidal deformability and $R_{1.4}$ (radius of NS with mass $1.4 M_{\odot}$) (Alam et al. 2016; Carson et al. 2019a,b). By obligating $K_{sym,0}$ in the befitting range we can measure tidal deformability theoretically, which is quite a complicated quantity to measure independently, precisely upto a certain level of accuracy. Q_{sym} being the most ambiguous quantity also shows entirely different behaviour for NL3 and G3 parameter set. For G3 it falls in the positive magnitude range while for NL3 it beholds the negative magnitude as the temperature increases. Although there is no reported constraint on $Q_{sym,0}$ till now, but we believe that since G3 parameter set satisfy all the desired results for other NM parameters, so it is obvious to assume it of the right kind. However, some predictions made on the basis of skyrme interactions supports the negative magnitude of skewness parameter (Tews et al. 2017), so it is difficult to state anything about Q_{sym} with certainty.

4 COOLING THROUGH NEUTRINO EMISSION

In this section, we provide an approach to study the thermal evolution of the newly born dense star through EOS. It is widely believed that the compact star formed just after the supernova explosion contains tantamount nucleons i.e. almost equal number of protons and neutrons (Lattimer & Prakash 2004). After that the process of cooling and neutronization (Lattimer & Prakash 2004; Østgaard 2001) happens slowly and finally it achieves the thermal stabilization and the beta equilibrium, which we call cold neutron star. The direct Urca processes $n \rightarrow p + e^- + \bar{\nu}_e$ and $p + e^- \rightarrow n + \nu_e$, governs the cooling of compact stars (Boguta 1981) through neutrino emission and requires a superthreshold proton fraction inside the super-dense star core to operate. To realize the effect of neutrino emissivity on cooling mechanism and EOS, we consider a degenerate dense matter containing nucleons (neutrons and protons) and the electrons at finite temperature, for which the Lagrangian is redefined as

$$\mathcal{L}_{total} = \mathcal{L} + \bar{\phi}(i\gamma_{\mu}\partial^{\mu} - m_e)\phi, \quad (31)$$

where \mathcal{L} is the Lagrangian defined in Eq. 1, m_e being the mass of electron and the last term represents the electrons contribution in the matter, which are considered to be non-interacting particles. Following the same procedure as defined in section 2, we will get the total energy density for this system

$$E_{total} = E + \frac{2}{(2\pi)^3} \int_0^{k_e} d^3k \mathcal{E}_e(k) [f_e(T) + \bar{f}_e(T)], \quad (32)$$

where E is the energy density defined in equation 20, k_e is the Fermi momentum of electron, f_e is the Fermi distribution of electron for finite temperature and \mathcal{E}_e is the energy of electron given by

$$\mathcal{E}_e = \sqrt{k_e^2 + m_e^2}. \quad (33)$$

We maintained the same number density for proton and electron i.e. $n_p = n_e$, to achieve charge neutrality in the described system.

The expression for the neutrino emissivity (Q) in high dense system was first estimated by Lattimer et. al. in non-relativistic manner (Lattimer et al. 1991). Since the movement of nucleons in compact star cores is relativistic, so the relativistic expression for neutrino emissivity was later calculated by L. B. Leinson and A. Perez. The non-relativistic emissivity is quite small than what is predicted by the relativistic formalism. The detailed explanations and the derivation for the formula of neutrino emissivity (Q) in relativistic framework and mean field approximation, which is used here can be found in the reference (Leinson 2002; Leinson & Párez 2001).

The formula for neutrino emissivity is given by (Leinson 2002)

$$Q = \frac{457\pi}{10080} G_F^2 C^2 T^6 \Theta(k_e + k_p - k_n) \left\{ \left(C_A^2 - C_V^2 \right) M_p^* M_n^* \mathcal{E}_e + \frac{1}{2} \left(C_V^2 + C_A^2 \right) \left[4 \mathcal{E}_n \mathcal{E}_p \mathcal{E}_e - (\mathcal{E}_n - \mathcal{E}_p) \left((\mathcal{E}_n + \mathcal{E}_p)^2 - k_e^2 \right) + C_V C_M \frac{\sqrt{M_p^* M_n^*}}{M} \left[2 (\mathcal{E}_n - \mathcal{E}_p) k_e^2 - \left(3 (\mathcal{E}_n - \mathcal{E}_p)^2 - k_e^2 \right) \mathcal{E}_e + C_A \left(C_V + 2 \frac{\sqrt{M_p^* M_n^*}}{M} C_M \right) (\mathcal{E}_n + \mathcal{E}_p) \left(k_e^2 - (\mathcal{E}_n + \mathcal{E}_p)^2 \right) + C_M^2 \frac{1}{4M^2} \left[8 M^*{}^2 (\mathcal{E}_n - \mathcal{E}_p) \left(k_e^2 - (\mathcal{E}_n - \mathcal{E}_p) \mathcal{E}_e \right) + \left(k_e^2 - (\mathcal{E}_n - \mathcal{E}_p)^2 \right) \left(2 \mathcal{E}_n^2 + 2 \mathcal{E}_p^2 - k_e^2 \right) \mathcal{E}_e - \left(k_e^2 - (\mathcal{E}_n - \mathcal{E}_p)^2 \right) (\mathcal{E}_n + \mathcal{E}_p) (2 \mathcal{E}_n - 2 \mathcal{E}_p - \mathcal{E}_e) \right] \right] \right\}, \quad (34)$$

where $G_F = 1.166 \times 10^{-11}$ MeV $^{-2}$ is the Fermi weak coupling constant, $C = 0.973$ is the Cabibbo factor, $C_V = 1$ and $C_A = 1.26$ are the vector and axial-vector constants respectively and the constant $C_M = 3.7$ represents the weak magnetism effects. The condition inevitable for Urca

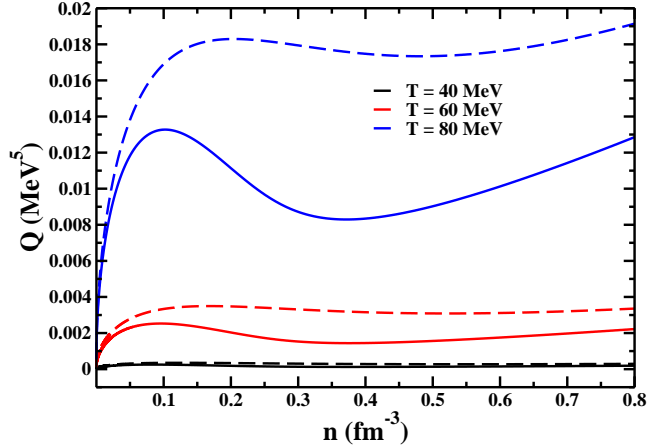


Figure 8. (colour online) Neutrino emissivity at different temperatures as a function of nucleon density for NL3 (solid line) and G3 (dashed line) parameter sets.

processes to go is represented by $\Theta(k_e + k_p - k_n) = 1$ if $k_e + k_p - k_n \geq 0$ and zero otherwise, where k_e , k_p and k_n are the Fermi momenta of electron, proton and neutron respectively.

Since, our defined system of nucleons and leptons (n-p-e) clearly satisfy the above necessary condition required for the initialisation of direct Urca process, so, we calculated the neutrino emissivity for both NL3 and G3 parameter sets which is displayed in Fig. 8. The dashed lines in the Fig. 8 represent the results for G3 and the solid lines stand for NL3 parameter. Some very interesting remarks can be concluded based on these curves of Q depicted at different temperatures. The most vital observation of this work is that the neutrino emissivity is responsible for cooling of newly born dense star only in its initial stage i.e. when the temperature is quite high and the neutrons are enough thermally excited to trigger the direct Urca process. As dense object cools down the magnitude of Q decreases substantially and then cooling mainly takes place through photon emission. This behaviour can be seen clearly in Fig. 8 for both G3 and NL3 parameters. The magnitude of Q for 40 MeV (represented by black line) temperature is negligible in comparison to 80 MeV curve (blue line). Also, initially the diffusion rate of neutrinos is so high that the matter cools down within a fraction of seconds and it is believed that it is so effective that it lowers the temperature to about 1 billion Kelvin during this momentary span (Yakovlev et al. 2011; Brown et al. 2018b). Another important dimension that we observe in this curve is the difference in the magnitude of the Q values for NL3 and G3 parameter sets. This tells us about the dependence (34) of cooling property of newly born star on the EoS. As we know that NL3 provides the stiffest EoS, which means the high mass of the proto-neutron star and G3 being the softer EoS in comparison to NL3 predicts lower mass. Keeping this fact in mind we concluded that the cooling of proto-neutron star through direct Urca process is slow in heavier star and fast in the lighter one.

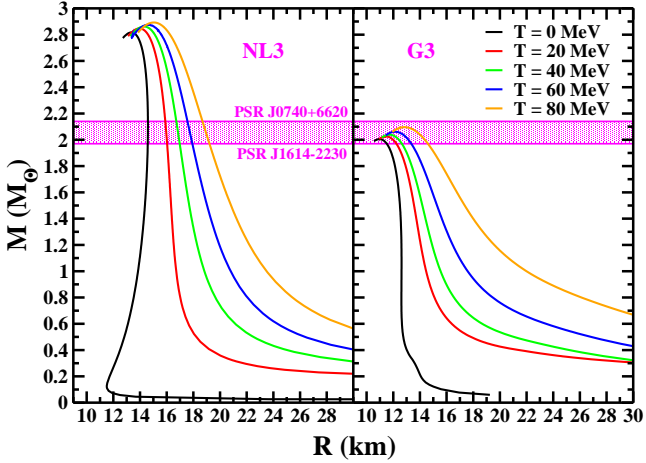


Figure 9. (colour online) M-R profile of proto-neutron star at different temperatures for NL3 (left panel) and G3 (right panel) parameter sets.

5 PROTO-NEUTRON STAR

To understand the complete penchant of temperature on a dense matter system, we performed a calculation to obtain the mass-radius (M-R) profile of proto-neutron star in this section. We took the Lagrangian mentioned in Eq. 31 into account to derive the EoS for the proto-neutron star system envisaged in the present section. We also maintained the necessary β - equilibrium and charge neutrality conditions i.e.

$$\mu_n = \mu_p + \mu_e, \quad (35)$$

$$n_p = n_e, \quad (36)$$

where μ_n , μ_p and μ_e are the chemical potentials of the neutron, proton and electron respectively; n_p and n_e are the number densities of proton and electron. By imposing the above stated conditions on the described Lagrangian, we can easily calculate the mass and radius of the static isotropic proto-neutron star using the Tolman-Oppenheimer-Volkov (TOV) equations (Tolman 1939; Oppenheimer & Volkoff 1939). The TOV equations are

$$\frac{dP(r)}{dr} = -\frac{[E(r) + P(r)][M(r) + 4\pi r^3 P(r)]}{r^2 \left(1 - \frac{2M(r)}{r}\right)}, \quad (37)$$

$$\frac{dM(r)}{dr} = 4\pi r^2 E(r), \quad (38)$$

These equations are integrated from $r = 0$ to the stellar surface $r = R$, where $P(R) = 0$, for a particular choice of central density $\rho_c = \rho(0)$ to determine the NS mass $M = M(R)$. The value of ρ_c that produces the maximum mass M_{max} for a given EoS is ρ_{max} . The neutrino free mass-radius profile of the proto-neutron star is plotted in Fig. 9. The results from the precisely measured neutron stars masses, such as PSR J1614-2230 with mass $M = 1.97 \pm 0.04 M_\odot$ (Demorest et al. 2010) and PSR J0740+6620 with $M = 2.15^{+0.10}_{-0.09} M_\odot$ (Cromartie et al. 2019) are shown in the horizontal bars in pink color. These observations suggest that the maximum mass predicted by any theoretical model should reach the limit $\sim 2.0 M_\odot$, and this condition is satisfied by

all of the EoSs taken into consideration. We notice that the inclusion of temperature increases the pressure at a given baryon density which yields the increase the mass-radius profile of the proto-neutron star. The proto-neutron star has a little-bit large mass compared with that of the neutron star at zero temperature because the EoS is stiffer in the former case.

6 SUMMARY AND CONCLUSIONS

We have studied the consequences of finite temperature on the nuclear properties of SNM and the crucial section required for the cooling of remnants of supernovae explosion. We used well known NL3 and the recently developed G3 parameter sets of the RMF model for a comparative study and concluded that NL3 with the possession of stiffest EoS does not provide the empirical values for most of the nuclear properties. The variations of the binding energy and pressure with baryon density for different temperatures are qualitatively similar for both the parameter sets. However, G3 predicts the higher value of critical temperature for liquid-gas phase transition, which is more proximate to the reported experimental values. We also observed a contrarious development in the value of K_0 for the defined parameter sets with increase of temperature. Both K and K_{sym} being the second derivatives of the different forms of energy, this behaviour of K_0 may be influenced by the magnitude of K_{sym} which is positive for NL3 and negative for the G3 parameter set. K_{sym} value of the G3 parameter set lies in the range reported by the NICER and LIGO collaboration. This result shows that the G3 parameter set is more suitable to reproduce the appropriate form of the EoS and can be used to study the properties of neutron stars more accurately. We did not observe any significant variation in the Q_{sym} parameter at saturation density for the G3 parameter set, while its value decreases for the NL3 parameter set.

We emphasized on the cooling mechanism of high dense matter and studied the effects of both the parameter sets on the neutrino emissivity. We used the relativistic approach to derive the detailed expression of neutrino emissivity, which is more effective than the non-relativistic approach. We concluded some important remarks about the cooling mechanism of the newly born proto-neutron star on the basis of the outcomes of our detailed calculation. We observed that the magnitude of neutrino emission is directly proportional to the temperature of the dense object. As the body cools down, the magnitude of the neutrino emission decreases. Also, the neutrino emissivity has maximum value around the saturation density, which indicates that the saturated matter cools more rapidly through direct Urca process. Another important aspect that we inspect is that the neutrino emissivity is higher for that parameter set which provides softer EoS. As we can see in the previous section that the stiff EoS measures higher mass NS, so we concluded that the lighter remnant of the supernovae explosion cools down more expeditiously through neutrino emissivity of the direct Urca process. Moreover, We look forward to see if any post-merger signal is explored observationally in near future by LIGO/VIRGO and NICER collaboration, which will help

us to comprehend finite temperature nuclear matter physics more appropriately and extensively. We also take notice that the mass numerated by the G3 parameter set for whole temperature range fits in the envelope determined by the GW170817 experimental data. Finally we adduced that G3 parameter set is more appropriate to study the properties of stellar objects through EoS.

7 ACKNOWLEDGEMENT

I am really thankful to thank Prof. Ang Li for her support and helpful suggestions during this work. This work is partially supported by National Natural Science Foundation of China Grant No. 11873040.

REFERENCES

Abbott B. P., et al., 2017, *Phys. Rev. Lett.*, 119, 161101
 Abbott B. P., et al., 2018, *Phys. Rev. Lett.*, 121, 161101
 Agrawal B. K., De J. N., Samaddar S. K., Centelles M., Viñas X., 2014, *EPJ A*, 50
 Aguirre R., 2012, *Phys. Rev. C*, 85, 014318
 Alam N., Agrawal B. K., Fortin M., Pais H., Providência C., Raduta A. R., Sulaksono A., 2016, *Phys. Rev. C*, 94, 052801
 Baldo M., Burgio G., 2016, *Progress in Particle and Nuclear Physics*, 91, 203a–258
 Boguta J., 1981, *Phys. Lett. B*, 106, 255
 Brown E. F., Cumming A., Fattoyev F. J., Horowitz C. J., Page D., Reddy S., 2018a, *Phys. Rev. Lett.*, 120, 182701
 Brown E. F., Cumming A., Fattoyev F. J., Horowitz C. J., Page D., Reddy S., 2018b, *Phys. Rev. Lett.*, 120, 182701
 Burrello S., Colonna M., Zheng H., 2019, *Frontiers in Physics*, 7, 53
 Burrows A., 2000, *Nature*, 403, 727
 Carson Z., Steiner A. W., Yagi K., 2019a, *Phys. Rev. D*, 99, 043010
 Carson Z., Steiner A. W., Yagi K., 2019b, *Phys. Rev. D*, 100, 023012
 Chen L.-W., Cai B.-J., Ko C. M., Li B.-A., Shen C., Xu J., 2009, *Phys. Rev. C*, 80, 014322
 Colgate S. A., White R. H., 1966, *ApJ*, 143, 626
 Cromartie H. T., et al., 2019, *Nature Astronomy*, 4, 72a–76
 Danielewicz P., Lacey R., Lynch W. G., 2002, *Science*, 298, 1592
 Demorest P. B., Pennucci T., Ransom S. M., Roberts M. S. E., Hessels J. W. T., 2010, *Nature*, 467, 1081a–1083
 Elliott J. B., Lake P. T., Moretto L. G., Phair L., 2013, *Phys. Rev. C*, 87, 054622
 FRIB, Whitepapers of the 2007 NSAC Long Range Plan Town Meeting, January, 2007, <https://www.aps.org/units/dnp/meetings/town.cfm>
 Facilities G.-S., <https://www.ganil-spiral2.eu/scientists/ganil-spiral-2-facilities/accelerators/>
 Fetter A. L., Walecka J. D., 1971, *Quantum Theory of Many-Particle Systems*. McGraw-Hill, <https://www.bibsonomy.org/bibtex/2a89d5cbb622c7993781f36e0bc77c51/broader>
 Gilmore G., 2004, *Science*, 304, 1915
 Goudarzi S., Moshfegh H., Haensel P., 2018, *Nucl. Phys. A*, 969, 206
 Gusakov, M. E. 2002, *A&A*, 389, 702
 Iglio J., et al., 2006, *Phys. Rev. C*, 74, 024605
 Kaminker, A. D. Haensel, P. Yakovlev, D. G. 2001, *A&A*, 373, L17
 Kumar B., Singh S., Agrawal B., Patra S., 2017, *Nucl. Phys. A*, 966, 197
 Kumar B., Patra S. K., Agrawal B. K., 2018, *Phys. Rev. C*, 97, 045806
 Käijper W. A., Wegmann G., Hilf E. R., 1974, *Annal. of Phys.*, 88, 454
 Lalazissis G. A., König J., Ring P., 1997, *Phys. Rev. C*, 55, 540
 Lattimer J. M., Prakash M., 2004, *Science*, 304, 536
 Lattimer J. M., Pethick C. J., Prakash M., Haensel P., 1991, *Phys. Rev. Lett.*, 66, 2701
 Leinson L., 2002, *Nucl. Phys. A*, 707, 543a–560
 Leinson L., Pálfrey A., 2001, *Phys. Lett. B*, 518, 15
 Li B.-A., Chen L.-W., Ko C. M., 2008, *Phys. Reports*, 464, 113
 Liu B., Greco V., Baran V., Colonna M., Di Toro M., 2002, *Phys. Rev. C*, 65, 045201
 Mekjian A., Lee S., Zamick L., 2005, *Phys. Lett. B*, 621, 239
 Mezzacappa A., 2005, *Annual Review of Nuclear and Particle Science*, 55, 467
 Oechslin, R. Janka, H.-T. Marek, A. 2007, *A&A*, 467, 395
 Ono A., Danielewicz P., Friedman W. A., Lynch W. G., Tsang M. B., 2003, *Phys. Rev. C*, 68, 051601
 Oppenheimer J. R., Volkoff G. M., 1939, *Phys. Rev.*, 55, 374
 Østgaard E., 2001, Internal structure of neutron stars, <https://ui.adsabs.harvard.edu/abs/2001ragt.meet...730>
 Ou L., Li Z., Zhang Y., Liu M., 2011, *Phys. Lett. B*, 697, 246a–250
 Prakash M., Bombaci I., Prakash M., Ellis P. J., Lattimer J. M., Knorren R., 1997, *Phys. Reports*, 280, 1
 Riley T. E., Watts A. L., Bogdanov S., et al. 2019, *The Astrophys. Journal*, 887, L21
 Ryden B., 2003, NEUTRON STARS, http://www.astronomy.ohio-state.edu/~ryden/ast162_5/notes21.html
 Sakuragi Y., 2016, *Progress of Theoretical and Experimental Physics*, 2016
 Schneider A. S., Roberts L. F., Ott C. D., O'Connor E., 2019, *Phys. Rev. C*, 100, 055802
 Sharma B. K., Pal S., 2010, *Phys. Rev. C*, 81, 064304
 Singh S. K., Biswal S. K., Bhuyan M., Patra S. K., 2014, *Phys. Rev. C*, 89, 044001
 Souliotis G. A., Shetty D. V., Keksis A., Bell E., Jandel M., Veselsky M., Yennello S. J., 2006, *Phys. Rev. C*, 73, 024606
 Stone J., Reinhard P.-G., 2007, *Progress in Particle and Nuclear Physics*, 58, 587a–657
 Takatsuka T., 1985, *Progress of Theoretical Physics*, 73, 1043
 Takatsuka T., 1996, *Progress of Theoretical Physics*, 95, 901
 Tan N. H., Loan D. T., Khoa D. T., Margueron J., 2016, *Phys. Rev. C*, 93, 035806
 Tews I., Lattimer J. M., Ohnishi A., Kolomeitsev E. E., 2017, *The Astrophys. Journal*, 848, 105
 Tolman R. C., 1939, *Phys. Rev.*, 55, 364
 Tsang M., Lynch W., Danielewicz P., Tsang C., 2019, *Phys. Lett. B*, 795, 533
 Typel S., 2018, *Particles*, 1, 3
 Wang P., 2000, *Phys. Rev. C*, 61, 054904
 Wang Y., Guo C., Li Q., Fálvre A. L., Leifels Y., Trautmann W., 2018, *Phys. Lett. B*, 778, 207
 Yakovlev D. G., Levenfish K. P., 1995, *aap*, 297, 717
 Yakovlev D. G., Pethick C. 2004, *Appl. Rev. of A&A*, 42, 169
 Yakovlev D. G., Ho W. C. G., Shternin P. S., Heinke C. O., Potekhin A. Y., 2011, *MNRAS*, 411, 1977
 Yang S., Zhang B. N., Sun B. Y., 2019a, *Phys. Rev. C*, 100, 054314
 Yang S., Zhang B. N., Sun B. Y., 2019b, *Phys. Rev. C*, 100, 054314
 Zhan W., Xu H., Sun Z., Xiao G., et al. 2006, *IJMP E*, 15, 1941
 Zimmerman J., Carson Z., Schumacher K., Steiner A. W., Yagi K., 2020, Measuring Nuclear Matter Parameters with NICER and LIGO/Virgo ([arXiv:2002.03210](https://arxiv.org/abs/2002.03210))